ISSN Online: 2821-1693

Transactions on Machine Intelligence

Journal Homepage: https://tmachineintelligence.ir/

Dynamic Modeling of Power Systems in the Presence of Solid Oxide Fuel Cells and Wind Turbines

A. Amini Badr [1,*]

[1] Assistant Professor, Department of Electrical Engineering, Sardroud Center, Tabriz Branch, Islamic Azad University, Tabriz, Iran

ARTICLE INFO

Article History:
Received 26 December 2024
Received in revised form 2 March 2025
Accepted 25 May 2025
Available online 4 June 2025

Keywords:
Power System Dynamics,
Small-Signal Stability,
Heffron–Phillips Model,
Wind Turbine, Fuel Cell

ABSTRACT

The increasing integration of renewable and low-emission energy technologies into modern power systems has introduced new dynamic interactions that can significantly affect power-system stability. In particular, the simultaneous operation of Solid Oxide Fuel Cell (SOFC) power plants and Doubly Fed Induction Generator (DFIG)-based wind turbines with conventional synchronous generators creates a hybrid generation structure whose small-signal dynamic characteristics require comprehensive investigation. This paper investigates the small-signal stability of a power system in which an SOFC power plant and a DFIG-based wind turbine operate in parallel with a synchronous generator. To this end, a comprehensive mathematical model of the SOFC generation unit and the DFIG-based wind turbine is developed and integrated into a single-machine infinite-bus (SMIB) power-system configuration. The resulting nonlinear dynamic model represents the principal interactions among the conventional synchronous generator, SOFC unit, wind-energy conversion system, and the associated control and electrical components. The mathematical models are subsequently linearized around a selected operating point to obtain an appropriate small-signal representation of the integrated system. Based on the linearized model, a modified Heffron–Phillips model corresponding to the proposed generation configuration is derived, providing a systematic framework for evaluating the dynamic behavior and stability characteristics of the system. Small-signal stability is then assessed by examining the effects of the integrated SOFC and DFIG units under different system parameters and operating conditions. The results indicate that the integration of these generation technologies can alter the dynamic stability characteristics of the power system in both favorable and unfavorable ways. The magnitude and direction of these effects depend strongly on system parameters and operating conditions, highlighting the importance of considering the dynamic interactions between conventional and emerging generation technologies when assessing power-system stability. The proposed modeling and analytical framework can provide a useful basis for stability assessment and for the coordinated integration of SOFC and DFIG-based generation into future power systems.

* Corresponding Author: Arman.Amini@iau.ac.ir
Assistant Professor, Department of Electrical Engineering, Sardroud Center, Tabriz Branch, Islamic Azad University, Tabriz, Iran

http://dx.doi.org/10.47176/TMI.2025.244842

1. INTRODUCTION

Power generation using fuel cells is associated with very low to zero emissions and relatively high efficiency (35–60%), and depending on the type of electrolyte, fuel cells are classified into different categories. Among them, high-temperature Solid Oxide Fuel Cells (SOFCs) are expected to have the greatest potential in the future as clean, grid-connected power generation units [1–3]. With the rapid development of fuel-cell generation technology, it is anticipated that, in the near future, the large-scale grid-connected operation of fuel-cell power plants will affect not only distribution networks, but also transmission systems and other generators. Therefore, the impact of renewable-based generation particularly large-scale fuel-cell units on the security and stability of future power systems must be carefully examined [5–10], including their influence on small-signal stability.

On the other hand, in recent years, wind turbine technology and installed capacity have grown significantly. Wind turbines may operate individually or as part of large wind farms. The response of wind turbines to grid disturbances especially with increasing penetration levels has become a critical issue. Thus, analyzing their behavior in the power grid is of great importance [11–16].

Several studies have investigated the impact of fuel-cell generators and wind power plants on power-system stability. In [5–7], the dynamic behavior of power systems in the presence of fuel-cell generators has been discussed. In [5], the structure of SOFC power plants is presented along with a simulation model. Reference [6] develops dynamic models of microturbines and fuel-cell units in distribution networks and demonstrates their effectiveness in assessing small-signal oscillations. Some of the earliest works on fuel-cell dynamic modeling and their impact on power-system control and stability can be found in [8, 9]. In [10], the effect of SOFC-based power generation operating alongside synchronous generators on small-signal stability is investigated.

Wind turbines with variable-speed operation extract approximately 2–6% more energy compared to fixed-speed turbines. In particular, DFIG-based wind turbines deliver approximately 20% and 60% more energy than variable-speed squirrel-cage induction generators and fixed-speed generators, respectively [11]. Hence, extensive research efforts have focused on DFIG-based systems [12–14,17]. In [14,17], the dynamic modeling of power systems with DFIG-based wind turbines has been presented. Reference [14] also proposes a control strategy to enhance voltage and frequency stability and examines small-signal stability. Moreover, the stability of renewable-based microgrids especially those integrating wind and solar energy has been studied in [18–20].

However, only a limited number of works have analyzed the combined impact of wind-power generation and fuel-cell penetration on overall power-system stability. Hybrid systems incorporating wind turbines and fuel cells have been dynamically evaluated in [21–23]. In [23], the fuel cell is considered as a backup source for wind turbines, and a control algorithm for optimal wind-energy utilization is proposed. In [24], a robust intelligent controller is introduced to enhance the stability of a grid-connected microgrid containing photovoltaic, wind, and fuel-cell generators. It is also worth noting that Heffron–Phillips linear models have been used for oscillation damping and optimal-controller design in [8, 25].

In this paper, a dynamic model of a power system incorporating a synchronous generator, a DFIG-based wind turbine, and an SOFC power plant is developed to investigate how the simultaneous operation of these units influences the small-signal stability of the grid. The main objective is to provide a clear representation of the stability characteristics induced by such hybrid power generation. To this end, a single-machine infinite-bus system equipped with an SOFC plant and a DFIG wind turbine is considered, assuming that their power capacity is comparable to that of the synchronous generator. This configuration may also represent future power systems where aggregated renewable or fuel-cell units supply significant portions of system load.

A complete mathematical representation of the integrated system is developed, and the corresponding Heffron–Phillips model incorporating both SOFC and wind-turbine subsystems is derived. Based on this model, the small-signal stability characteristics of the system are then analyzed.

Section 2 presents the structure and modeling of the SOFC and wind-turbine generators and the associated power-system model, along with linearization of the overall system. Simulation studies and analysis of the obtained results are provided in Section 3, while Section 4 concludes the paper.

2. GENERATOR MODELING OF THE SYSTEM

Figure 1 illustrates the structure of a simplified single-machine power system with an infinite bus, to which the wind turbine (WT) and solid oxide fuel cell (SOFC) generators are connected. In this system, the reactances، X_{sb} ، X_{cs}،X_{fs} , X_{ts} and X_{wt} represent the equivalent reactances of the transformers and the transmission line.

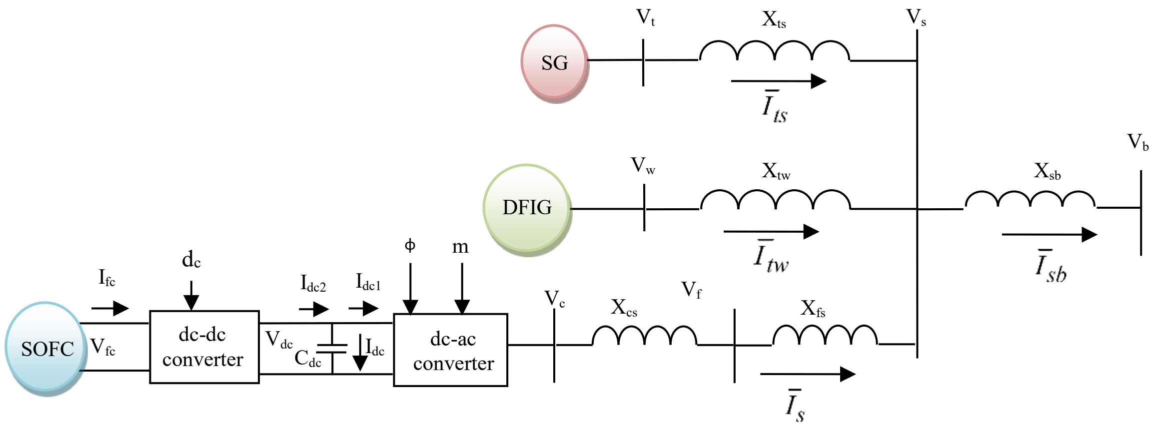

Fig. 1. Configuration of WT and SOFC connection to a single-machine power system with an infinite bus

2.1. Synchronous Generator Model

The mathematical model of the synchronous machine can be expressed as $\dot{X}_g = F(X_g, \bar{I}_{ts})$, where $X_g$is the state-variable vector associated with the dynamic states of the generator, as presented in Equations (1)–(4). The variable $\bar{I}_{ts}$represents the coupling current between the generator and the remainder of the system.

In the $d-q$ reference frame of the generator, $\bar{I}_{ts}$can be expressed in terms of its d- and q-axis components, denoted by $i_{tsd}$and i_{tsq}, respectively. In this paper, a synchronous generator model suitable for small-signal stability analysis of power systems is employed [24].

$$\dot{\delta} = \omega_0(\omega - 1) \tag{1}$$

$$\dot{\omega} = \frac{1}{M}[P_m - P_t - D(\omega - 1)] \tag{2}$$

$$\dot{E}_q^{'} = \frac{1}{T_{do}^{'}}(-E_q + E_{fd}) \tag{3}$$

$$\dot{E}_{fd}^{'} = -\frac{1}{T_A}E_{fd}^{'} + \frac{K_A}{T_A}(V_{tref} - V_t) \tag{4}$$

Assuming $X_g = \begin{bmatrix} \delta & \omega & E_q^{'} & E_{fd}^{'} \end{bmatrix}^T$ Equations (5)–(7) are obtained.

$$P_t = E_q^{'} i_{tsq} + (x_q - x_d^{'})\, i_{tsd}\, i_{tsq} \tag{5}$$

$$E_q = E_q^{'} - (x_d - x_d^{'})\, i_{tsd} \tag{6}$$

$$V_t = \sqrt{v_{td}^2 + v_{tq}^2} = \sqrt{(x_q\, i_{tsq})^2 + (E_q^{'} - x_d^{'}\, i_{tsd})^2} \tag{7}$$

V_t denotes the terminal voltage of the synchronous generator, $E_q'$is the internal voltage behind the generator's transient reactance, $x_d$is the d-axis reactance, and $x_q$is the q-axis reactance.

2.2. SOFC Power Plant Modelling

Figure 2 presents the block diagram of the SOFC generator, and its dynamic model is subsequently described in this section [5–10].

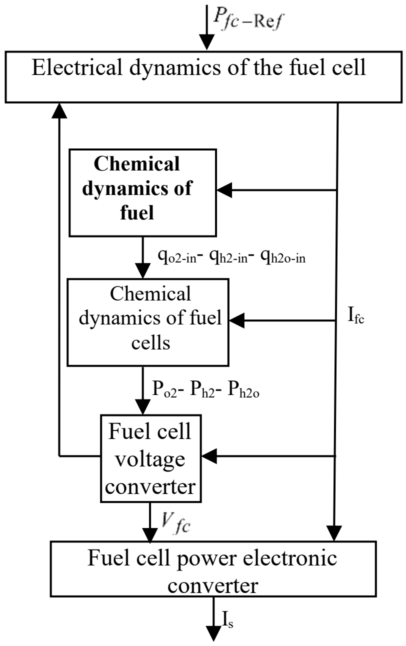

Fig. 2. SOFC box diagram

The electrical dynamics, control process, and output current of the fuel cell, I_{fc}, are described by Equation (8):

$$I_{fc-ref} = \frac{P_{fc-ref}}{V_{fc}} \tag{8}$$

where P_{fc}denotes the fuel cell power. A first-order transfer function with a time constant of approximately 0.08 s is employed to model its dynamic behavior.

$$I_{fc} = \frac{1}{1+T_e s} I_{fc-ref} \tag{9}$$

The fuel supply dynamics, referred to as the *fuel processing dynamics*, are represented by a first-order transfer function describing the transient behavior of the fuel feed system. The chemical dynamics of the fuel cell characterize the electrochemical reaction processes occurring within the fuel cell stack and are modeled by three first-order transfer functions corresponding to hydrogen, oxygen, and water, respectively. The output voltage of the fuel cell converter is given by Equation (10):

$$V_{fc} = N_0 \left[E_0 + \frac{RT}{2F} ln\left(\frac{p_{h2} \times p_{o2}^{0.5}}{p_{h2o}}\right)\right] - rI_{fc} \tag{10}$$

where $E_0$is the ideal standard potential, $N_0$is the number of cells connected in series, $R$is the universal gas constant, $T$is the absolute temperature, and $r$denotes the ohmic losses. The SOFC power plant consists of a DC–DC converter, a DC–AC converter, and their corresponding controllers. Regulation of the fuel cell output current is achieved through control of the DC–DC converter.

$$d_c = d_{c0} + T_{dc}(s)(I_{fc-ref} - I_{fc}) \quad (11)$$

where $d_c$is the duty cycle and $T_{dc}(s)$denotes the transfer function of the fuel cell current controller. In the $d-q$ reference frame of the generator, the AC voltage at the terminal of the DC–AC converter can be expressed as in Equation (12).

$$\bar{V}_c = mkV_{dc}(\cos\psi + j\sin\psi) = mkV_{dc}\angle\psi \quad (12)$$

where $k$is the converter ratio, which is assumed to be 0.75. The parameters $m$and φ represent the modulation index and the phase angle of the PWM control algorithm of the DC–AC converter, respectively. The active power delivered from the SOFC power plant to the grid is given by:

$$V_{dc}I_{dc1} = i_{sd}v_{cd} + i_{sq}v_{cd} = i_{sd}mkV_{dc}\cos\psi + i_{sq}mkV_{dc}\sin\psi \quad (13)$$

where $i_{sd}$and $i_{sq}$are the d- and q-axis components of $\bar{I}_s$, and $v_{cd}$and $v_{cq}$are the d- and q-axis components of $\bar{V}_s$, respectively. The active power of the SOFC power plant is expressed by Equation (14).

$$P_{fc} = I_{fc}V_{fc} = I_{dc2}V_{dc} \quad (14)$$

The dynamic equation of the DC–AC converter is given by:

$$\dot{V}_{dc} = \frac{1}{C_{dc}}I_{dc} = \frac{1}{C_{dc}}(I_{dc2} - I_{dc1}) = \frac{1}{C_{dc}}\left[P_{fc}/V_{dc} - (i_{sd}mk\cos\psi + i_{sq}mk\sin\psi)\right] \quad (15)$$

To stabilize the DC voltage across the capacitor, a voltage controller is employed, and typically the modulation index is controlled to regulate the AC voltage amplitude.

2.3. Wind Turbine (WT) Modeling Considering DFIG

In dynamic stability studies, machines are generally modeled as voltage sources connected to a transient impedance [25]. Accordingly, the equivalent circuit of the doubly fed induction generator (DFIG) is shown in Figure 3.

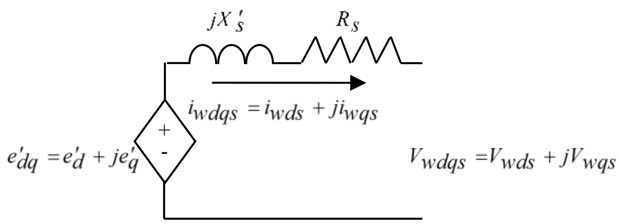

Fig. 3. Dynamic model of the DFIG

By expressing the relationship between the stator voltage and current in terms of the voltage applied to the transient impedance, as well as the stator and rotor current equations in the dqreference frame, the DFIG model can be formulated as follows. The algebraic equations of the DFIG are obtained directly from the dynamic equivalent circuit of the machine:

$$e'_d - V_{wds} - R_s i_{wds} + X'_s i_{wqs} = 0 \quad (16)$$

$$e'_q - V_{wqs} - R_s i_{wqs} - X'_s i_{wds} = 0 \quad (17)$$

In the above equations, I_w denotes the wind turbine current, X' the transient reactance, $X$the reactance, T_0' the transient time constant, e' the internal voltage behind the transient reactance, and $\omega$the angular velocity.

Considering the configuration shown in Figure 1 and working in the $d-q$ reference frame, Equations (18) and (19) can be derived.

$$\begin{bmatrix} x_{sb} & x_s + x_{sb} & x_{sb} \\ x_{sb} & x_{sb} & x_{sb} + x_{tw} \\ x_q + x_{ts} + x_{sb} & x_{sb} & x_{sb} \end{bmatrix} \begin{bmatrix} i_{tsq} \\ i_{sq} \\ i_{wq} \end{bmatrix} = \begin{bmatrix} V_b \sin\delta - V_c \cos\psi \\ V_b \sin\delta - V_{dw} \\ V_b \sin\delta \end{bmatrix} \tag{18}$$

$$\begin{bmatrix} x_{sb} & x_s + x_{sb} & x_{sb} \\ x_{sb} & x_{sb} & x_{sb} + x_{tw} \\ x_d' + x_{ts} + x_{sb} & x_{sb} & x_{sb} \end{bmatrix} \begin{bmatrix} i_{tsd} \\ i_{sd} \\ i_{wd} \end{bmatrix} = \begin{bmatrix} V_c \sin\psi - V_b \cos\delta \\ V_{qw} - V_b \cos\delta \\ E_q' - V_b \cos\delta \end{bmatrix} \tag{19}$$

In this manner, the mathematical model corresponding to Figure 1 is obtained. This model comprises the generator model, the fuel cell model, the wind turbine model, and the power system network model.

The linearization of the resulting equations is presented in the following. The linearized form of Equation (12) is given by $\Delta V_c = k(m_0\, \Delta V_{dc} + V_{dc0}\, \Delta m)$. Accordingly, the linearized forms of Equations (18) and (19) are obtained as follows:

$$\begin{bmatrix} \Delta i_{tsd} \\ \Delta i_{sd} \\ \Delta i_{wd} \end{bmatrix} = B^{-1} \begin{bmatrix} k \sin\psi_0\, (m_0\, \Delta V_{dc} + V_{dc0} \Delta m) + V_b \sin\delta_0\, \Delta\delta + V_{c0} \cos\psi_0\, \Delta\psi \\ V_b \sin\delta_0\, \Delta\delta + \Delta e_q' + x_s' \Delta i_{ds} \\ \Delta E_q' + V_b \sin\delta_0\, \Delta\delta \end{bmatrix} \tag{20}$$

$$\begin{bmatrix} \Delta i_{tsq} \\ \Delta i_{sq} \\ \Delta i_{wq} \end{bmatrix} = A^{-1} \begin{bmatrix} -k \cos\psi_0\, (m_0\, \Delta V_{dc} + V_{dc0} \Delta m) + V_b \cos\delta_0\, \Delta\delta + V_{c0} \sin\psi_0\, \Delta\psi \\ V_b \cos\delta_0\, \Delta\delta - (\Delta e_d' + x_s' \Delta i_{qs}) \\ V_b \cos\delta_0\, \Delta\delta \end{bmatrix} \tag{21}$$

where the matrices $A^{-1}$and $B^{-1}$are given in Equations (22) and (23), respectively.

$$A^{-1} = \frac{\begin{bmatrix} -x_{sb}x_{tw} & -x_s x_{sb} & x_s x_{sb} + x_{tw} x_s + x_{sb} x_{tw} \\ x_{sb}x_q + x_{sb}x_{ts} + x_q x_{tw} + x_{tw} x_{ts} + x_{tw} x_{sb} & -(x_q + x_{ts}) x_{sb} & -x_{tw} \\ -x_{sb}(x_q + x_{ts}) & x_s x_q + x_s x_{ts} + x_{sb} x_s + x_{sb} x_{ts} & -x_s x_{sb} \end{bmatrix}}{(x_s x_{sb} + x_{tw} x_s + x_{sb} x_{tw})(x_q + x_{ts}) + x_{sb} x_s x_{tw}} \tag{22}$$

$$B^{-1} = \frac{\begin{bmatrix} -x_{sb}x_{tw} & -x_s x_{sb} & x_s x_{sb} + x_{tw} x_s + x_{sb} x_{tw} \\ x_{sb}x_d' + x_{sb}x_{ts} + x_d' x_{tw} + x_{tw} x_{ts} + x_{tw} x_{sb} & -(x_d' + x_{ts}) x_{sb} & -x_{sb} x_{tw} \\ -x_{sb}(x_d' + x_{ts}) & x_s x_d' + x_s x_{ts} + x_{sb} x_s + x_{sb} x_d' + x_{sb} x_{ts} & -x_s x_{sb} \end{bmatrix}}{(x_s x_{sb} + x_{tw} x_s + x_{sb} x_{tw})(x_d' + x_{ts}) + x_{sb} x_s x_{tw}} \tag{23}$$

Assuming that the state-variable vector is given by:

$X = [\Delta\delta \quad \Delta E_q' \quad \Delta V_{dc} \quad \Delta m \quad \Delta\psi \quad \Delta i_{ds} \quad \Delta i_{qs} \quad \Delta e_d' \quad \Delta e_q']^T$, Equations (22) and (23) can be rewritten in terms of the state variables as follows:

$$\begin{bmatrix} \Delta i_{tsq} \\ \Delta i_{sq} \\ \Delta i_{wq} \end{bmatrix} = A^{-1} \begin{bmatrix} V_b \cos\delta_0 & 0 & -k \cos\psi_0\, m_0 & -k \cos\psi_0\, V_{dc0} & V_{c0} \sin\psi_0 & 0 & 0 & 0 & 0 \\ V_b \cos\delta_0 & 0 & 0 & 0 & 0 & 0 & -x_s' & -1 & 0 \\ V_b \cos\delta_0 & 0 & 0 & 0 & 0 & 0 & 0 & 0 & 0 \end{bmatrix} X \tag{24}$$

$$\begin{bmatrix}\Delta i_{tsd}\\ \Delta i_{sd}\\ \Delta i_{wd}\end{bmatrix} = B^{-1}\begin{bmatrix}V_b \sin\delta_0 & 0 & k\sin\psi_0\, m_0 & k\sin\psi_0\, V_{dc0} & V_{c0}\cos\psi_0 & 0 & 0 & 0 & 0\\ V_b\sin\delta_0 & 0 & 0 & 0 & 0 & -x_s' & 0 & 0 & 1\\ V_b\sin\delta_0 & 1 & 0 & 0 & 0 & 0 & 0 & 0 & 0\end{bmatrix} X \tag{25}$$

By linearizing the equations associated with the SOFC, Equations (29)–(31) are obtained:

$$\Delta\dot{V}_{dc} = \frac{-1}{C_{dc}}\left(\frac{P_{fc0}}{V_{dc0}^2}\Delta V_{dc} + f_1\Delta i_{sd} + f_2\Delta i_{sq} + f_3\Delta m + f_4\Delta\psi\right) \tag{26}$$

$$\Delta\phi = T_{vdc}(s)\Delta V_{dc} \tag{27}$$

$$\Delta m = T_{vac}(s)\Delta V_s \tag{28}$$

where $T_{vdc}(s)$and $T_{vac}(s)$denote the transfer functions of the DC- and AC-voltage controllers, respectively. The linearized model of the voltage $V_s$is expressed in Equation (29):

$$\Delta V_s = B_1\Delta\delta + B_2\Delta E_q' + B_{dc}\Delta V_{dc} + B_3\Delta m + B_4\Delta\psi + B_5\Delta i_{wds} + B_6\Delta i_{wqs} + B_7\Delta e_d' + B_8\Delta e_q' \tag{29}$$

Therefore, Equation (28) can be represented in the form of Equation (30):

$$\Delta m = T_{vac}(s)(B_1\Delta\delta + B_2\Delta E_q' + B_{dc}\Delta V_{dc} + B_3\Delta m + B_4\Delta\psi + B_5\Delta i_{wds} + B_6\Delta i_{wqs} + B_7\Delta e_d' + B_8\Delta e_q') \tag{30}$$

By linearizing the equations associated with the wind turbine, the following relations are obtained:

$$\Delta i_{wds} = \frac{\omega_s}{X_s'}\left\{\frac{ci}{cb_{66}}b_{61}\Delta\delta + \frac{ci}{cb_{66}}b_{62}\Delta E_q' + \frac{ci}{cb_{66}}b_{63}\Delta V_{dc} + \frac{ci}{cb_{66}}b_{64}\Delta m + \frac{ci}{cb_{66}}b_{65}\Delta\psi + \left(\frac{ci}{cb_{66}}b_{67} + X_s'\right)\Delta i_{wqs} + \left[\frac{ci}{cb_{66}}b_{68} - (1-s_r)\right]\Delta e_d' + \left[\frac{ci}{cb_{66}}\left(b_{69} + \frac{1}{\omega_s L_m}\right) + \frac{1}{\omega_s T_0'}\right]\Delta e_q'\right\} \tag{31}$$

$$\Delta i_{wqs} = \frac{\omega_s}{X_s'}\left\{\frac{ci}{cb37}b_{31}\Delta\delta + \frac{ci}{cb_{37}}b_{32}\Delta E_q' + \frac{ci}{cb37}b_{33}\Delta V_{dc} + \frac{ci}{cb_{37}}b_{34}\Delta m + \frac{ci}{cb_{37}}b_{35}\Delta\psi + \left(\frac{ci}{cb37}b_{36} - X_s'\right)\Delta i_{wds} + \left[\frac{ci}{cb_{37}}\left(b_{38} + \frac{1}{\omega_s L_m}\right) - \frac{1}{\omega_s T_0'}\right]\Delta e_d' + \left[\frac{ci}{cb37}b_{39} - (1-s_r)\right]\Delta e_q'\right\} \tag{32}$$

$$\Delta e_d' = \frac{1}{\frac{1}{T_0'}+s}\left[s_{r0}\omega_s\Delta e_q' - \frac{1}{T_0'}(X_s - X_s')\Delta i_{wqs}\right] \tag{33}$$

$$\Delta e_q' = \frac{1}{\frac{1}{T_0'}+s}\left[-s_{r0}\omega_s\Delta e_d' + \frac{1}{T_0'}(X_s - X_s')\Delta i_{wds}\right] \tag{34}$$

In the above relations, $c_i = -R_s - \frac{1}{\omega_s T_0'}(X_s - X_s'), c_{b66} = \left(1 - \frac{L_m}{L_{rr}}\right) - b_{66}, c_{b37} = \left(1 - \frac{L_m}{L_{rr}}\right) - b_{37}$ Considering Equations (20) and (21) and the linearization of Equations (5)–(7), the dynamic equations of the generator can be expressed as follows:

$$\Delta\delta' = \omega_0\Delta\omega \tag{35}$$

$$\Delta\dot{\omega} = \frac{1}{M}(-D\Delta\omega - K_1\Delta\delta - K_2\Delta E_q' - K_{pdc}\Delta V_{dc} - K_{pm}\Delta m - K_{p\psi}\Delta\psi - K_{pds}\Delta i_{wds} - K_{pqs}\Delta i_{wqs} - K_{ped}\Delta e_d' - K_{peq}\Delta e_q') \tag{36}$$

$$\Delta\dot{E}_q' = \frac{1}{T_{do}'}(\Delta E_{fd}' - K_4\Delta\delta - K_3\Delta E_q' - K_{qdc}\Delta V_{dc} - K_{qm}\Delta m - K_{q\psi}\Delta\psi - K_{qds}\Delta i_{wds} - K_{qqs}\Delta i_{wqs} - K_{qed}\Delta e_d' - K_{qeq}\Delta e_q') \tag{37}$$

$$\Delta\dot{E}'_{fd} = -\frac{1}{T_A}\Delta E'_{fd} - \frac{K_A}{T_A}(K_5\Delta\delta + K_6\Delta E'_q + K_{vdc}\Delta V_{dc} + K_{vm}\Delta m + K_{v\psi}\Delta\psi + K_{vds}\Delta i_{wds} + K_{vqs}\Delta i_{wqs} + K_{ved}\Delta e'_d + K_{veq}\Delta e'_q) \tag{38}$$

Accordingly, the linearized system model is obtained and can be represented as shown in Figure 4. It can be observed that Figure 4 corresponds to a Heffron–Phillips model. In this model, the subsystems of the fuel cell power plant and the wind turbine, along with their corresponding Kcoefficients, are incorporated. The coefficients of this model are derived from the linearized equations and the unique characteristics of each system.

Furthermore, the wind turbine and fuel cell power plants influence the electromechanical oscillation loop of the synchronous generator both directly and indirectly, and the electrical torque can be decomposed into two components: the synchronizing torque and the damping torque.

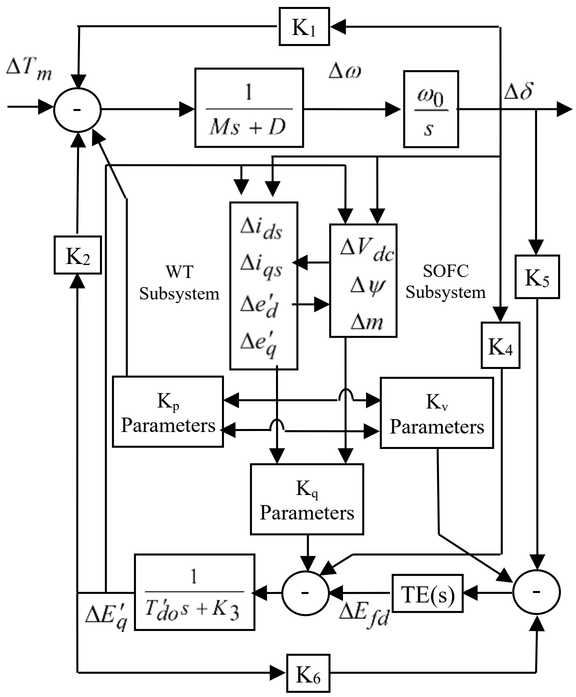

Fig. 4. Linearized power system model considering SOFC and WT

3. SIMULATION AND SMALL-SIGNAL STABILITY ANALYSIS

Eigenvalue analysis is an effective method for investigating power system stability, as it is based on the linearized system model. Accordingly, the system analysis in this section is performed using this approach. The values of the variables related to the fuel cell generator and the wind turbine are provided in Appendix C. The system simulation was carried out using MATLAB, and the eigenvalue loci of the system are shown in Figure 5.

As observed in Figures 5(b) and 5(c), all system eigenvalues are located on the left-hand side of the $j\omega$ axis. Additionally, the eigenvalues, oscillation frequencies, and damping ratios are listed in Table 1.

Table 1. System Eigenvalues

Eigenvalue	Oscillation Frequency (Hz)	Damping Ratio
-8.716	0	1
-1.245	0	1
-0.977	0	1
-0.0003 ± 0.98i	0.16	0.0003
-0.113 ± 0.215i	0.03	0.46
-0.09	0	1
-0.002	0	1
-0.002 ± 0.23i	0.03	0.01

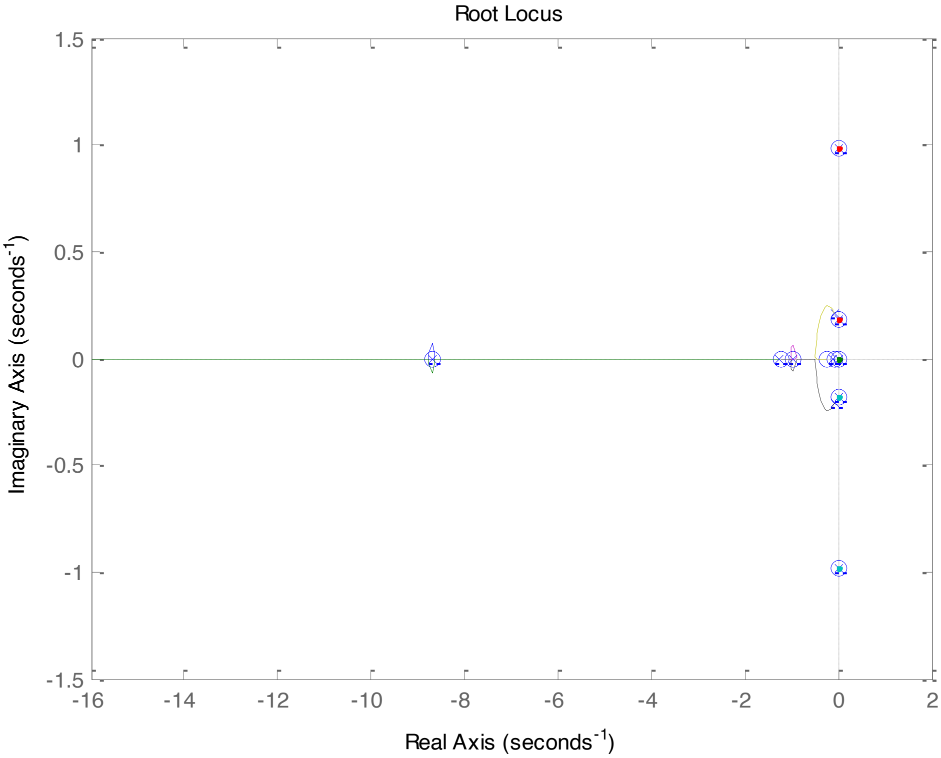

(a)

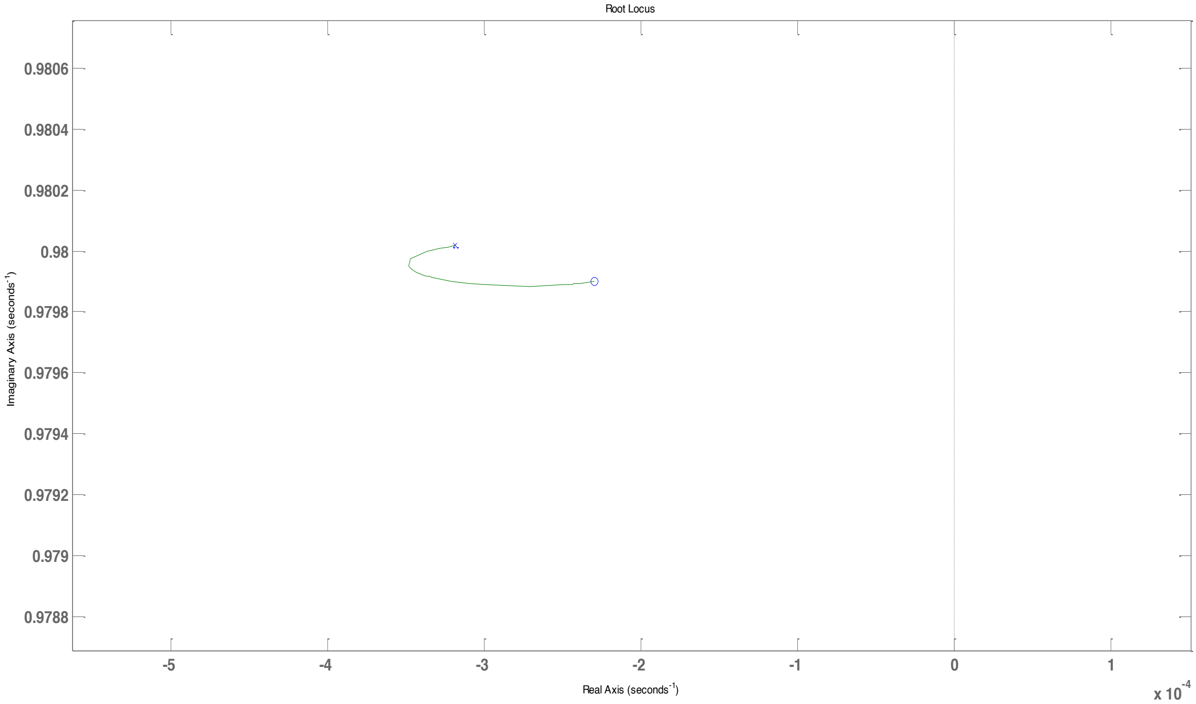

(b)

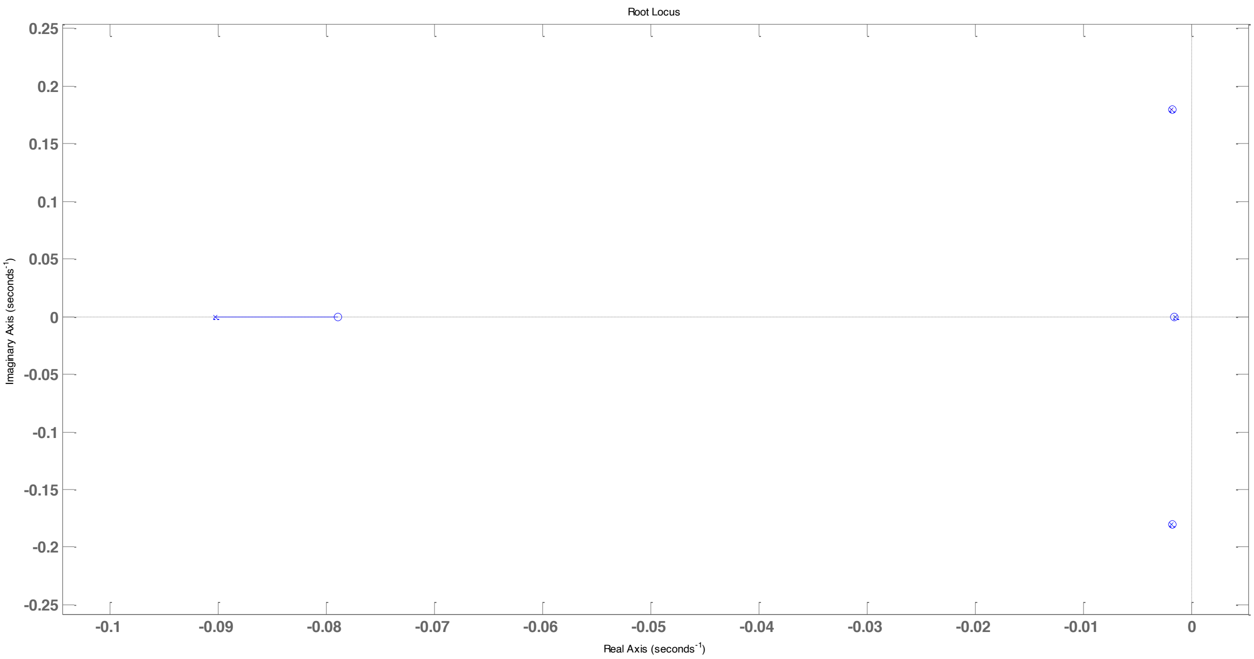

(c)

Fig. 5. Eigenvalue loci of the system

In this section, the effects of variations in the transmission line reactance and the fuel cell voltage angle (ψ) on the small-signal response of the power system are examined. The transmission network reactance is considered to be 0.1 p.u. for the strong system and 1 p.u. for the weak system, and the corresponding dynamic system response is obtained. Figures 6 and 7 illustrate the variations in rotor angle and electrical power in response to changes in the transmission line reactance.

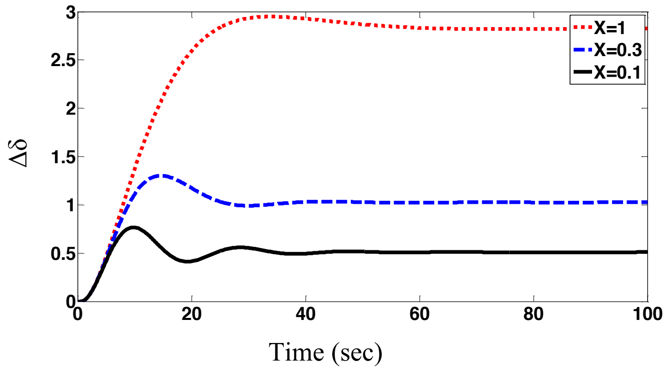

Fig. 6. Rotor angle deviation: solid line $X_{sb} = 0.1$, dashed line $X_{sb} = 0.3$, dotted line $X_{sb} = \mathbf{1}$

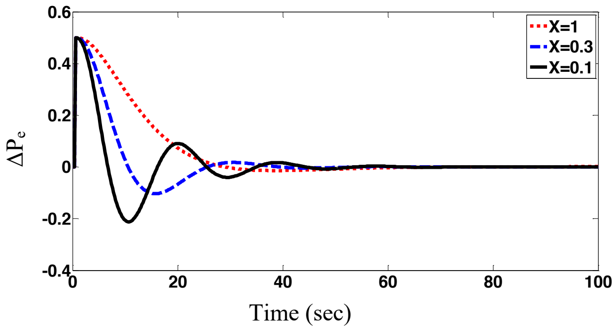

Fig. 7. Deviation of output electrical power: solid line $X_{sb} = 0.1$, dashed line $X_{sb} = 0.3$, dotted line $X_{sb} = 1$

Figures 8 and 9 show the system response for different values of ψ, and Table 2 presents the oscillatory modes of the system. Based on the results, it can be observed that when the angle $\psi$is 40°, the system becomes unstable, whereas for values in the range of 60° to 80°, the system remains stable under small-signal disturbances.

Table 2. Oscillatory modes for different values of ψ

$\lambda_{3,4}$	$\lambda_{1,2}$	(°)ψ
-0.076 ± 0.19i	**±0.98i**	**40**
-0.09 ± 0.2i	**-0.0002 ± 0.19i**	**60**
-0.1 ± 0.21i	**-0.0003 ± 0.98i**	**80**

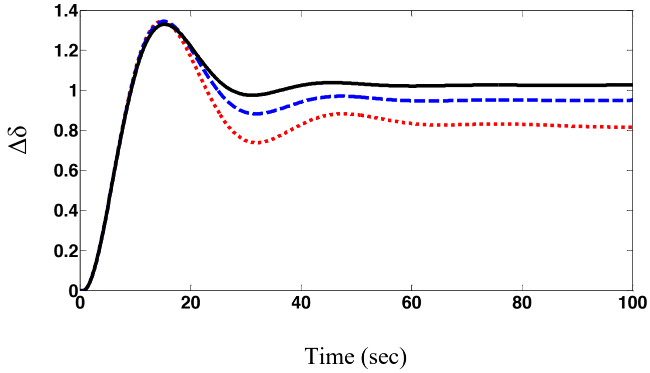

Fig. 8. Rotor angle deviation: solid line $\psi = 80°$, dashed line $\psi = 60°$, dotted line $\psi = 40°$

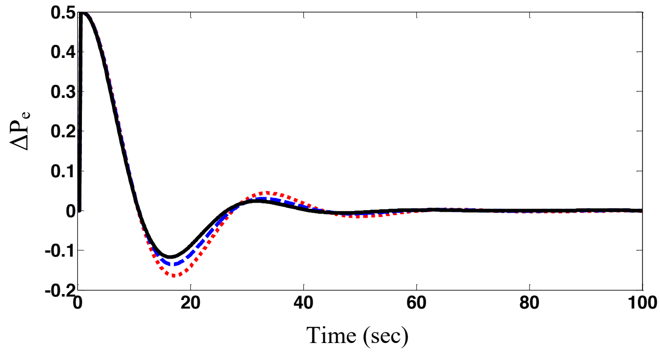

Fig. 9. Deviation of output electrical power: solid line $\psi = 80°$, dashed line $\psi = 60°$, dotted line $\psi = 40°$

4. CONCLUSION

In this paper, the dynamic model of a power system in the presence of SOFC fuel cell and DFIG wind turbine generators was developed. The linearized models of the fuel cell and wind turbine were derived separately, and their corresponding coefficients were determined. Based on this, a Heffron–Phillips linear model incorporating the subsystems of these generators was presented. The proposed model is useful and effective for dynamic and small-signal stability studies in power systems with renewable energy-based generators. Using this model, the system eigenvalues can be computed, and the effects of various network parameters on the small-signal stability of the system can be analyzed, demonstrating its applicability.

Declaration

We acknowledge that we used ChatGPT to enhance the academic writing of our manuscript while ensuring the originality and integrity of our work.

Transparency Statement

The data supporting this study are available upon reasonable request to the corresponding author, subject to ethical and confidentiality considerations.

Acknowledgments

We would like to express our gratitude to all individuals who contributed to this project.

Declaration of Interest

The authors declare that they have no competing interests.

Funding

This research received no specific grant from any funding agency, commercial, or not-for-profit sectors.

REFERENCES

[1] Thounthong, P., Davat, B., Rael, S., & Sethakul, P. (2009). Fuel cell high-power applications. *IEEE Industrial Electronics Magazine, 3*(1), 33–46. https://doi.org/10.1109/MIE.2008.930365

[2] Yu, S., Fernando, T., Chau, T. K., & Iu, H. H. C. (2017). Voltage control strategies for solid oxide fuel cell energy system connected to complex power grids using dynamic state estimation and STATCOM. *IEEE Transactions on Power Systems, 32*(4), 3136–3145. https://doi.org/10.1109/TPWRS.2016.2615075

[3] Li, Y. H., Rajakaruna, S., & Choi, S. S. (2007). Control of a solid oxide fuel cell power plant in a grid-connected system. *IEEE Transactions on Energy Conversion, 22*(2), 405–413. https://doi.org/10.1109/TEC.2005.853756

[4] Yu, S., Fernando, T., & Iu, H. H. (2016). Dynamic behaviour study and state estimator design for solid oxide fuel cells in hybrid power systems. *IEEE Transactions on Power Systems, 31*(6), 5190–5199. https://doi.org/10.1109/TPWRS.2016.2525782

[5] Padulles, J., Ault, G. W., & McDonald, J. R. (2000). An integrated SOFC plant dynamic model for power systems simulation. *Journal of Power Sources, 86*(1–2), 495–500. https://doi.org/10.1016/S0378-7753(99)00430-9

[6] Zhu, Y., & Tomsovic, K. (2002). Development of models for analyzing the load following performance of micro turbines and fuel cells. *Electric Power Systems Research, 62*(1), 1–11. https://doi.org/10.1016/S0378-7796(02)00033-0

[7] Georgakis, D., Papathanassiou, S., & Manias, S. (2005). Modeling and control of a small-scale grid-connected PEM fuel cell system. In *Proceedings of the IEEE 36th Power Electronics Specialists Conference* (pp. 1614–1620). IEEE. https://doi.org/10.1109/PESC.2005.1581846

[8] Sedghisigarchi, K., & Feliachi, A. (2004). Dynamic and transient analysis of power distribution systems with fuel cells Part I: Fuel-cell dynamic model. *IEEE Transactions on Energy Conversion, 19*(2), 423–428. https://doi.org/10.1109/TEC.2004.827039

[9] Sedghisigarchi, K., & Feliachi, A. (2004). Dynamic and transient analysis of power distribution systems with fuel cells Part II: Control and stability enhancement. *IEEE Transactions on Energy Conversion, 19*(2), 429–434. https://doi.org/10.1109/TEC.2003.822302

[10] Du, W., Wang, H. F., Zhang, X. F., & Xiao, L. Y. (2012). Effect of grid-connected solid oxide fuel cell power generation on power systems small-signal stability. *IET Renewable Power Generation, 6*(1), 24–37. https://doi.org/10.1049/iet-rpg.2010.0024

[11] Chatterjee, S., Naithani, A., & Mukherjee, V. (2016). Small-signal stability analysis of DFIG-based wind power system using teaching learning based optimization. *International Journal of Electrical Power & Energy Systems, 78*, 672–689. https://doi.org/10.1016/j.ijepes.2015.11.113

[12] Wu, F., Zhang, X. P., Godfrey, K., & Ju, P. (2007). Small signal stability analysis and optimal control of a wind turbine with doubly fed induction generator. *IET Generation, Transmission & Distribution, 1*(5), 751–760. https://doi.org/10.1049/iet-gtd:20060395

[13] Zaminifar, M., Fani, B., Golshan, M. E. H., & Karshenas, H. R. (2014). Dynamic modeling and optimal control of DFIG wind energy systems using DFT and NSGA-II. *Electric Power Systems Research, 108*, 50–58. https://doi.org/10.1016/j.epsr.2013.10.021

[14] Geng, H., Xi, X., & Yang, G. (2017). Small signal stability of power system integrated with ancillary controlled large scale DFIG-based wind farm. *IET Renewable Power Generation, 11*(8), 1191–1198. https://doi.org/10.1049/iet-rpg.2016.0078

[15] Catalán, P., Wang, Y., Arza, J., & Chen, Z. (2023). A comprehensive overview of power converter applied in high-power wind turbine: Key challenges and potential solutions. *IEEE Transactions on Power Electronics, 38*, 6169–6195. https://doi.org/10.1109/TPEL.2023.3234221

[16] Narula, A., Imgart, P., Bongiorno, M., Beza, M., Svensson, J. R., & Hasler, J. P. (2023). Voltage-based current limitation strategy to preserve grid-forming properties under severe grid disturbances. *IEEE Open Journal of Power Electronics, 4*, 176–188. https://doi.org/10.1109/OJPEL.2023.3246728

[17] Bhushan, R., & Chatterjee, K. (2017). Effects of parameter variation in DFIG-based grid-connected system with a FACTS device for small-signal stability analysis. *IET Generation, Transmission & Distribution, 11*(11), 2762–2777. https://doi.org/10.1049/iet-gtd.2016.1329

[18] Krismanto, A., Mithulananthan, N., & Lee, K. Y. (2015). Comprehensive modeling and small signal stability of RES-based micro-grid. *IFAC-PapersOnLine, 48*(13), 282–287. https://doi.org/10.1016/j.ifacol.2015.12.391

[19] Kabalci, E. (2013). Design and analysis of a hybrid renewable energy plant with solar and wind power. *Energy Conversion and Management, 72*, 51–59. https://doi.org/10.1016/j.enconman.2012.08.027

[20] Rajesh, K., Kulkarni, A. D., & Ananthapadmanabha, T. (2015). Modeling and simulation of solar PV and DFIG-based wind hybrid system. *Procedia Technology, 21*, 667–675. https://doi.org/10.1016/j.protcy.2015.10.080

[21] Iqbal, M. T. (2003). Modeling and control of a wind fuel cell hybrid energy system. *Renewable Energy, 28*(2), 223–237. https://doi.org/10.1016/S0960-1481(02)00016-2

[22] Khan, M. J., & Iqbal, M. T. (2005). Dynamic modeling and simulation of a small wind-fuel cell hybrid energy system. *Renewable Energy, 30*(3), 421–439. https://doi.org/10.1016/j.renene.2004.05.013

[23] Bizon, N. (2018). Optimal operation of fuel cell/wind turbine hybrid power system under turbulent wind and variable load. *Applied Energy, 212*, 196–209. https://doi.org/10.1016/j.apenergy.2017.12.034

[24] Chuang, S. J., Hong, C. M., & Chen, C. H. (2016). Design of intelligent control for stabilization of micro-grid system. *International Journal of Electrical Power & Energy Systems, 82*, 569–578. https://doi.org/10.1016/j.ijepes.2016.04.030

[25] Safari, A., & Shayeghi, H. (2009). Optimal design of UPFC-based damping controller using iteration, PSO. *World Academy of Science, Engineering and Technology, 3*(4), 709–714.

[26] Yu, Y. N. (1983). *Electric power system dynamics*. Academic Press.

[27] Kundur, P. (1994). *Power system stability and control*. McGraw-Hill.